

ACTIVE MEDIA

PACS numbers: 42.70.Hj; 81.05.Je; 71.36.+c
DOI: 10.1070/QE2012v042n10ABEH014920

Structural features of dielectric oxide laser ceramics

A.A. Kaminskii, A.V. Taranov, E.N. Khazanov, M.Sh. Akchurin

Abstract. **The relation between the transport characteristics of subterahertz thermal phonons and the structural features of single-phase dielectric crystalline laser ceramics based on cubic oxides synthesised in different technological regimes is studied. The effect of plastic deformation on the formation of the grain structure and intergrain layers (boundaries), as well as on the thermophysical, acoustic, optical, and laser characteristics of the materials is analysed.**

Keywords: *laser ceramics, phonons, intergrain boundary, twinning.*

A.A. Kaminskii, M.Sh. Akchurin A.V. Shubnikov Institute of Crystallography, Russian Academy of Sciences, Leninskii prosp. 59, 119333 Moscow, Russia
A.V. Taranov, E.N. Khazanov V.A. Kotel'nikov Institute of Radio Engineering and Electronics, Russian Academy of Sciences, ul. Mokhovaya 11, bldg. 7, 125009 Moscow, Russia;
e-mail: taranov@cplire.ru

Received 8 June 2012; revision received 15 August 2012
Kvantovaya Elektronika **42** (10) 880–886 (2012)
Translated by M.N. Basieva

5. Introduction

One of the important achievements of the last decade in laser physics, as well as in solid-state physics and optical materials science is the creation of a new class of active functional materials – laser crystalline ceramics based on cubic oxides doped with trivalent lanthanide ions Ln^{3+} [1–5]. The scale of these achievements is demonstrated in Table 1, which lists the most well-known ceramics.

Investigations showed that the laser characteristics of ceramics strongly depend on the size and structure of their crystallites (grains) and developed system of intergrain layers (boundaries). It was also found that the thermal conduction of ceramics and single crystals of the same composition at $T \geqslant 300$ K is almost identical, while the mechanical characteristics (hardness) of ceramics are noticeably better than those of single crystals. This is especially pronounced in the case of the widely used laser ceramics based on the $Y_3Al_5O_{12}$ garnet oxide (see, for example, [35]). The motivation of this paper, which is devoted mainly to this garnet ceramics, can be under-

Table 1. Dielectric laser ceramics, active Ln^{3+} ions, and stimulated radiation (SR) channels.

Crystalline ceramics	Space group	Ln^{3+} laser ions and SR channels					
		Pr^{3+}	Nd^{3+}	Ho^{3+}	Er^{3+}	Tm^{3+}	Yb^{3+}
				Oxide			
Sc_2O_3	$T_h^7 - Ia\bar{3}$	–	–	–	$^4I_{13/2} \rightarrow {}^4I_{15/2}$ [6]	–	$^2F_{5/2} \rightarrow {}^2F_{7/2}$ [7]
Y_2O_3	$T_h^7 - Ia\bar{3}$	–	$^4F_{3/2} \rightarrow {}^4I_{11/2}$ [8]	$^5I_7 \rightarrow {}^5I_8$ [9]	$^4I_{13/2} \rightarrow {}^4I_{15/2}$ [10] $^4I_{11/2} \rightarrow {}^4I_{13/2}$ [11]	–	$^2F_{5/2} \rightarrow {}^2F_{7/2}$ [12]
Y_2O_3–ThO_2	$T_h^7 - Ia\bar{3}$	–	$^4F_{3/2} \rightarrow {}^4I_{11/2}$ [13]	–	–	–	–
$\{Y_3\}[Al_2](Al_3)O_{12}$	$O_h^{10} - Ia\bar{3}d$	–	$^4F_{3/2} \rightarrow {}^4I_{9/2}$ [14] $^4F_{3/2} \rightarrow {}^4I_{11/2}$ [15] $^4F_{3/2} \rightarrow {}^4I_{13/2}$ [16]	$^5I_7 \rightarrow {}^5I_8$ [17]	$^4I_{13/2} \rightarrow {}^4I_{15/2}$ [18]	$^3H_4(^3F_4) \rightarrow {}^3H_6$ [19]	$^2F_{5/2} \rightarrow {}^2F_{7/2}$ [20]
$\{Y_3\}[Al_{0.5}Sc_{0.5}](Al_3)O_{12}$	$O_h^{10} - Ia\bar{3}d$	–	$^4F_{3/2} \rightarrow {}^4I_{11/2}$ [21]	–	–	–	$^2F_{5/2} \rightarrow {}^2F_{7/2}$ [22]
$\{YGd_2\}[Sc_2](Al_2Ga)O_{12}$	$O_h^{10} - Ia\bar{3}d$		–	–	–	–	$^2F_{5/2} \rightarrow {}^2F_{7/2}$ [23]
$\{Y_{0.5}Er_{0.5}\}[Al_2](Al_3)O_{12}$	$O_h^{10} - Ia\bar{3}d$	–	–	–	$^4I_{11/2} \rightarrow {}^4I_{13/2}$ [24] $^4S_{3/2} \rightarrow {}^4I_{9/2}$ [5]	–	–
$(Y_{0.5}Gd_{0.5})_2O_3$	$T_h^7 - Ia\bar{3}$	–	$^4F_{3/2} \rightarrow {}^4I_{11/2}$ [25]	–	–	–	–
$Ba(Mg,Zr,Ta)O_3$	$O_h^5 - Fm\bar{3}m$	–	$^4F_{3/2} \rightarrow {}^4I_{11/2}$ [26]	–	–	–	–
Lu_2O_3	$T_h^7 - Ia\bar{3}$	–	$^4F_{3/2} \rightarrow {}^4I_{11/2}$ [27]	–	–	$^3H_4(^3F_4) \rightarrow {}^3H_6$ [28]	$^2F_{5/2} \rightarrow {}^2F_{7/2}$ [29]
$\{Lu_3\}[Al_2](Al_3)O_{12}$	$O_h^{10} - Ia\bar{3}d$	–	–	–	–	–	$^2F_{5/2} \rightarrow {}^2F_{7/2}$ [30]
				Fluoride			
CaF_2–SrF_2–YbF_3	$O_h^5 - Fm\bar{3}m$						$^2F_{5/2} \rightarrow {}^2F_{7/2}$ [31]
SrF_2	$O_h^5 - Fm\bar{3}m$	$^3P_0 \rightarrow {}^3F_2$ [32]	$^4F_{3/2} \rightarrow {}^4I_{11/2}$ [33]				
				Oxyfluoride			
$Ca_5(PO_4)_3F$	$C_{6h}^2 - P6_3/m$		$^4F_{3/2} \rightarrow {}^4I_{11/2}$ [34]				

Note: The table is based on pioneering papers published in peer-reviewed scientific journals.

stood from the data of Fig. 1, which demonstrates the evolution of the output powers of $Y_3Al_5O_{12}$ laser ceramics achieved for the years of its investigation and application and shows that the output power was increased from 70 mW in the first experiments to more than 100 kW in recently developed lasers. So that Fig. 1 was not overloaded with references, we give the results of only several key works, which determined this progress. Other key laser publications are described in sufficient detail in some reviews (see, for example, [1–5]). To be fair, we should also mention the paper on the spectroscopy of $Nd^{3+}:Y_3Al_5O_{12}$ ceramics published in 1990 [40] and one of the authors of this work, T. Yanagitani, who, together with the scientists of Konoshima Chemical, developed the leading-edge vacuum sintering and nanocrystalline (VSN) technology of fabrication of highly transparent $Nd^{3+}:Y_3Al_5O_{12}$ laser ceramics [41]. All the achievements shown in Fig. 1 beginning from 2000 belong to the ceramics produced by this Japan company.

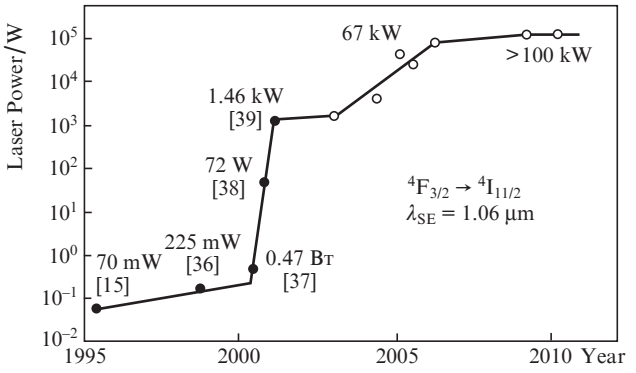

Figure 1. 15-year evolution of achievements in the development of diode-pumped $Y_3Al_5O_{12}:Nd^{3+}$ ceramic lasers. The illustrative dependence of the output power is plotted based on the data from [3, 5]. The open circles show achievements reported at conferences (according to [5]).

As will be shown below, the main requirements to these materials (absence of stresses in grains, homogeneous distribution of the dopant, fast heat removal from the lasing region) are controlled by the grain structure and the quality of interface layers in the region of their contact. At present, the problem of improvement of ceramics quality consists in the optimisation of the grain structure and size, as well as of the conditions of formation of contact boundaries. The character and structure of boundaries in a specified volume are analysed by high-resolution transmission electron microscopy. These investigations confirm the existence of continuous intergrain layers with a thickness of several nanometers [42]. At the same time, electron and atomic-force microscopies can analyse only limited volumes and do not allow one to make conclusions on the average characteristics of intergrain boundaries and their relation to the thermophysical, acoustic, and optical characteristics of materials [43].

An efficient method of investigating materials with structural defects is the heat pulse method [44]. At a decreased phonon temperature (energy), which creates conditions for competition between the times of elastic (τ_0) and inelastic (τ^*) phonon scattering, there exists a wide set of phonon transport regimes [45]. The most informative regime for investigating the structural defects and phonon transport processes is the classical diffusion regime, when a heat pulse is elastically scattered by the structural defects in the absence of inelastic phonon–phonon interactions. The condition for the occurrence of this regime for a time $t < \tau^*$ is the relation $\tau_0 \ll \tau_b \ll \tau^*$ (τ_b is the time of ballistic phonon transport). These conditions are fulfilled at liquid helium temperatures (2–4 K) almost for all dense oxide ceramics. In this case, the phonon wavelengths $\lambda_{ph} \approx 10-50$ nm are comparable with the characteristic sizes of the structural elements of ceramics (intergrain layers, pores, nanofragments of another phase).

The temperature dependences of the transport characteristics of subterahertz phonons in the diffusion regime at liquid helium temperatures were studied in [45]. Under these conditions, inelastic phonon–phonon processes can be neglected, and the elastic phonon scattering efficiency is determined only by the structural features of the material. Heating the metal film of the injector to a temperature T_h such that $\Delta T = T_h - T_0 \ll T_0$, one can study the temperature dependences of scattering by changing the thermostat temperature T_0. The signal recorded by a superconducting bolometer at the sample face opposite to the injector is well described by the solution of the diffusion equation. The experimentally measured value is the instant of recording of the diffusion signal maximum $t_{max} = L^2/2D(T)$ (plane source), where $D(T) = lv/3$, L is the sample size, D is the diffusion coefficient, l is the phonon free path, and v is the polarisation-averaged velocity of acoustic waves.

The authors of [46] showed that the frequencies of elastically scattered phonons forming the maximum of the diffusion signal recorded by a bolometer correspond to the energies $\hbar\omega \approx (3-4)k_BT$ (k_B is the Boltzmann constant), which allows one to consider the phonon transport within the single-frequency model. In experiments on thermal conductivity, phonons with these frequencies determine the temperature dependence of the thermal conductivity coefficient $K(T) = c_V D(T) \sim T$ in the temperature range from 8 to 16 K, which was observed in [47] for ceramics based on the $Y_3Al_5O_{12}$ garnet oxide.

The possibility of obtaining the phonon diffusion regime in ceramics in the region of liquid helium temperatures is shown in [48]. The method is sensitive to insignificant variations in the ceramics structure and allows one to estimate the acoustic impedance and the thickness of intergrain boundaries averaged over the sample volume [49].

The aim of this work is the study and optimisation of the grain structure and intergrain boundaries of the samples of crystalline laser ceramics based on $Nd^{3+}:Y_3Al_5O_{12}$ in order to improve the acoustic, thermophysical, and laser characteristics.

6. Structure of intergrain layers

In dense microstructured ceramics in the region of liquid helium temperatures, when the condition $qR \gg 1$ (q is the phonon wave vector and R is the average grain size) is fulfilled, the phonon spectrum is similar to the spectrum of vibrational excitations of grains, and the intergrain boundaries can be represented as plane layers of a finite thickness d with an acoustic impedance different from the impedance of the grain material [49]. If the phonon free path in ceramics is $l \gg R$, then we can assume that the intergrain boundaries are the main factor determining phonon scattering. In this case, the phonon transport mechanism can be represented as ballistic propagation of phonons in a grain with the probability f_ω of their transfer to the neighbouring grain.

In the diffusion regime for the time scale $t \gg t_0$ (t_0 is the time of the presence of a phonon in the grain), the diffusion

coefficient is $D \sim R^2/t_0$, where $t_0 \sim R(vf_\omega)^{-1}$. The value f_ω is determined as the ratio of the flux density of nonequilibrium phonons passing from one grain to another to the density of the flux incident to the boundary [49]. Then, $D \sim Rvf_\omega$, from which we conclude that, within the proposed model, $D \sim R$, and the spectral characteristics of phonons, i.e., $D(T)$, are determined by f_ω.

Figure 2 shows the dependences of the diffusion coefficient on the average number of grains in a series of ceramics (including optically transparent) based on cubic oxides at $T = 3.8$ K in the region of $qR \gg 1$. The variable parameters were the annealing temperature and time, which determined the average size of grains. The dependence $D(R)$ is close to linear within a range of R varying by 2–3 orders of magnitude. This fact testifies that the properties of intergrain layers remain stable in a wide range of technological parameters. The data presented in Fig. 2 point to a higher phonon diffusion coefficient in $Nd^{3+}:Y_3Al_5O_{12}$ ceramics than in $Y_3Al_5O_{12}$ ceramics, which, according to the model of [49], can be related to a higher density of intergrain layers due to sinking of heavier Nd^{3+} ions to the region of boundaries. Considering the spectral characteristics of the diffusion coefficient, we can expect a resonance character of the dependence f_ω, when the projection of the phonon wave vector is commensurable with the intergrain layer thickness. Under the conditions of our experiment, this may lead to a change of the sign of the derivative $\partial t_{max}/\partial T$ and, hence, of $\partial D/\partial T$.

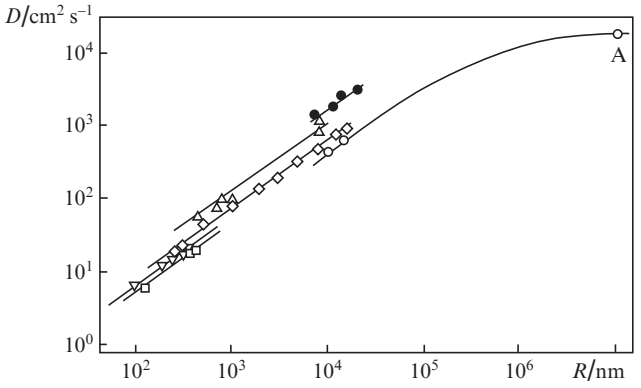

Figure 2. Dependences $D(R)$ in the region $qR \gg 1$ at $T = 3.8$ K in oxide ceramics Al_2O_3 [49] (◇); $ZrO_2:Y_2O_3$ [50] (□), $Y_2O_3:Nd^{3+}$ [51] (△), TiO_2 (microwave synthesis) [52] (▽); $Y_3Al_5O_{12}$ (○) and $Y_3Al_5O_{12}:Nd^{3+}$ ($C_{Nd} \approx 1\%$) [53] (●). The solid curves connect the experimental points for ceramic samples of identical compositions. Point A corresponds to the data for $Y_3Al_5O_{12}$ single crystal [46].

The method of determination of the acoustic impedance and thickness of intergrain layers based on the analysis of the temperature dependences $D(T)$ is described in [50] on the example of refining of different methods of compaction and synthesis of $ZrO_2:Y_2O_3$ ceramics. The experimental results were compared with the data calculated by the expression $l = l_0 f_\omega/(1 - f_\omega)$ [54], where l is the effective free path of phonons in a layered periodic structure with a period R in the absence of phonon scattering in the grain material. The phonon mean free path in a grain before the scattering event at the boundary is $l_0 = 0.6R$ [55].

Figure 3 shows the theoretical dependence of the ratio $l/l_0 = f_\omega/(1 - f_\omega)$ on the parameter q_2d (q_2 is the phonon wave vector in the intergrain layer material) in the samples of transparent optical ceramics $Nd^{3+}:Y_3Al_5O_{12}$. This dependence is the left trailing edge of the resonance curve for phonon scattering from a layer of a finite thickness d with an acoustic impedance different from the acoustic impedance of the grain material. The presented results correspond to the case when the impedance ratio of the grain material ($\rho = 4.55$ g cm^{-3}, $v = 5.6\times10^5$ cm s^{-1}) and the layer material (SiO_2 glass phase, $\rho_2 = 2.02$ g cm^{-3}, $v = 4.05\times10^5$ cm s^{-1}) is $z_2/z_1 = 0.32$. The inset shows the experimental dependences $D(T)$ for the studied samples. The phonon free path for a particular temperature was calculated from the values $t_{max}(T)$ by the formula $l(T) = 3L^2/[2vt_{max}(T)]$. From the value l/l_0 for one of the points (for example, $T = 3.8$ K), from the point of intersection with the theoretical dependence we determined the parameter q_2d, from which, in turn, we calculated the thickness d. The coordinates of the other points of the temperature dependence $D(T)$ for a given sample were the corresponding experimental values $l(T)/l_0$ and $q_2(T)d$ (for d calculated at the previous step). The points corresponding to the experimental data for all the samples lie on the calculated dependence, which testifies to a satisfactory quality of the proposed model. In the general case, when one has no idea on the intergrain layer material, the dependence $l(T)/l_0$ is put into correspondence with the curve of the most similar shape from the family of the theoretical dependences $f_\omega/(1 - f_\omega)$ for different ratios of the acoustic impedances of the grain and the intergrain layer. According to our estimates, the intergrain layer thickness d in the studied samples lies in the range from 0.21 to 0.45 nm.

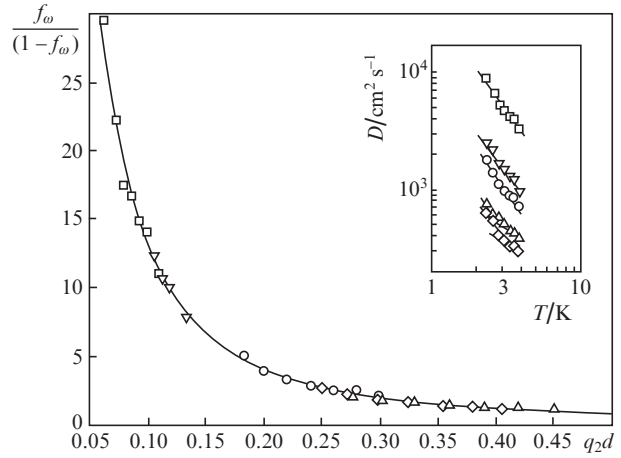

Figure 3. Calculated dependence $f_\omega/(1 - f_\omega)$ on the q_2d for $Y_3Al_5O_{12}:Nd^{3+}$ ($C_{Nd} = 1\%$) samples with $L = 0.108$ cm and $R = 22$ μm (◇), $L = 0.141$ cm and $R = 31$ μm (△), $L = 0.143$ cm and $R = 30$ μm (○), $L = 0.175$ cm and $R = 11$ μm (▽), and $L = 0.44$ cm and $R = 27$ μm (□) [56]. The inset shows experimental data.

In $Nd^{3+}:Y_2O_3$ and Lu_2O_3 ceramics synthesised in the absence of SiO_2 [51, 57], the estimated intergrain layer thicknesses were close to the lattice constant of the grain material. The principal distinction of the samples of ceramics synthesised by the VSN method was the presence of twins in the grain structure.

Figure 4 shows the images of triple junctions observed on an etched surface (a) and a fracture (b) of a sample of $Y_3Al_5O_{12}$ ceramics. The junction angles of 120° testify to ordering of the grain structure, since cubic structures can form crystallographic boundaries of this configuration only when the grains

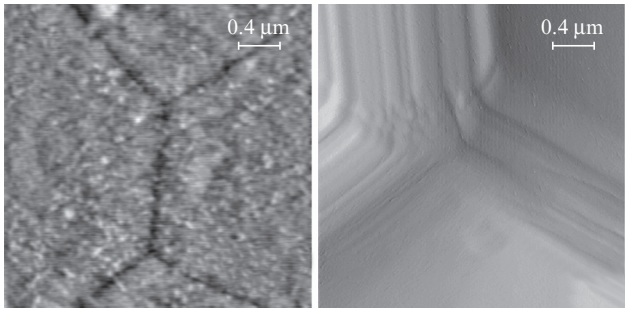

Figure 4. AFM images of triple junctions on etched surfaces (a) and fractions (b) of an $Y_3Al_5O_{12}$ ceramic sample.

are bound by 111 planes. Twinning in the interface regions of grains (Fig. 4b) also points to the existence of natural crystallographic boundaries. A model of formation and shift of twin boundaries and of healing of pores by rotating a part of the structure around the threefold axis by 60° is presented in papers [35, 58–60].

7. Specific features of the kinetics of subterahertz phonons in ceramics with twinning elements in the structure

Even the first investigations of the structure of intergrain boundaries in $Y_3Al_5O_{12}$ ceramics (Konoshima Chemical Co.) [53] revealed that the intergrain boundaries in all samples are well stabilised and their average thicknesses are smaller than the lattice constant of the grain material (a = 1.202 nm). This was responsible for the good optical and thermophysical properties of the samples. Paper [47] published the data on the thermal conductivity in $Y_3Al_5O_{12}$ ceramics with the grain size R = 4–5 μm and an order of magnitude larger free path of phonons in the region of liquid helium temperature. These data indirectly point to advanced technological procedures, which allowed the authors to improve the material structure, which contradicts the assumption on intergrain layers of a finite thickness.

The experimental kinetic characteristics of phonons at T = 3.86 K in $Y_3Al_5O_{12}$ ceramic samples taken from [60] are given in Table 2.

The maximum free path was observed in sample 1. Comparable phonon free paths under the same experimental conditions were observed in single crystal of 15–20-percent solid solutions $(Y_{1-c}Ln_c)_3Al_5O_{12}$ [46]. Analysing the kinetic characteristics and the structures of the first and the last samples in Table 2, one can see some distinctions correlating with the grain size. Investigations of the fractures of samples by scanning and atomic force microscopies showed that twinning in samples with R = 1–2 μm occurred over the entire volume. The distance between the twinning planes was ∼100 nm (Fig. 5a). At $R > 2$ μm, twinning was either observed only in the region of boundaries or was not observed at all (Fig. 5b).

There is a set of results on an increase in the number of defects and stresses induced by them in the structure of grains with their growth. In particular, destruction of samples with a grain size of 1–2 μm occurs mainly along the grain boundaries. In ceramics with a large grain size ($R \geqslant 10$ μm), mainly the grains themselves are destroyed. This fact testifies to a lower hardness and to existence of stresses in the structure of large

Table 2. Kinetic characteristics of phonons in $Y_3Al_5O_{12}$ ceramic samples at T = 3.86 K [60].

Sample number	L/cm	R/μm	D/cm^2 s^{-1}	l/cm	l/R
1	0.31	1	4.41×10^3	2.36×10^{-2}	236
2	0.9	7	2.37×10^3	1.27×10^{-2}	18
3	0.31	6.5	1.46×10^3	0.78×10^{-2}	12
4	0.31	6.5	1.25×10^3	0.67×10^{-2}	10.3
5	0.145	13.5	0.86×10^3	0.46×10^{-2}	3.4
6	0.16	11	5.6×10^3	0.3×10^{-2}	2.95
7	0.24	1–2	1.5×10^3	0.8×10^{-2}	54
8	–	3	–	1×10^{-2}	25
9	–	4	–	0.75×10^{-2}	25
10	–	7.5	–	1.5×10^{-2}	20
11	0.175	11	0.96×10^3	0.51×10^{-2}	4.6
12	0.44	27	3.2×10^3	1.73×10^{-2}	5.76
13	0.143	30	0.73×10^3	0.39×10^{-2}	1.3

Note. Samples 1–10 are produced by Konoshima Chemical Co.: (1–3) $Nd^{3+}:Y_3Al_5O_{12}$, (4–7) $Y_3Al_5O_{12}$ [53]; and (8–10) $Y_3Al_5O_{12}$ [47]. (11–13) are $Nd^{3+}:Y_3Al_5O_{12}$ samples from Institute of Radio Engineering and Electronics, Russian Academy of Sciences [56].

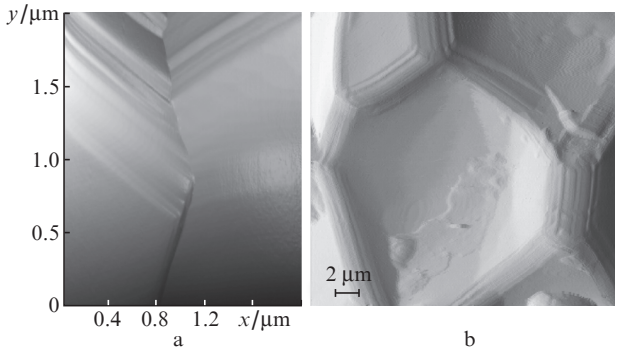

Figure 5. Microphotographs of fractures along grain boundaries (a) and through a grain (b) of ceramic samples.

grains. The problem of structural defects, stresses caused by these defects, and grain anisotropy still remains open. The optical anisotropy of ∼5% in neighbouring grains was observed in the process of annealing of samples of Y_2O_3 ceramics [61].

Figure 6 shows the asymptotics of the trailing edge of the diffusion signal $S(t)$ for some samples from Table 2. The dependence $S(t) \sim t^{-1/2}$ observed in samples 1 and 7 was typi-

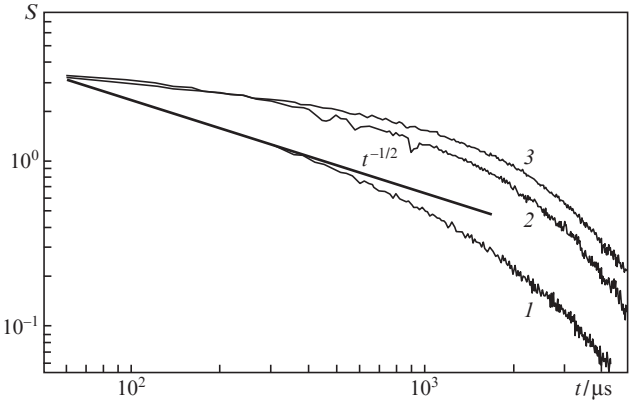

Figure 6. Asymptotics of the trailing edges of diffusion signals recorded by a bolometer for samples 1 (*1*), 3 (*2*), and 12 (*3*) from Table 2.

cal for the conditions of classical diffusion and a plane source of phonons. The asymptotics of the trailing edge of signals in samples 3 and 12 ($R > 10$ μm) showed a pulling of the signal, which may be related to the reflection of phonons from the boundaries due to the anisotropy of neighbouring grains. Another indirect evidence of an increase in the number of defects and corresponding stresses with increasing grain size ($R \geqslant 10$ μm) is the behaviour of the dependence of l/R on the grain size (Fig. 7).

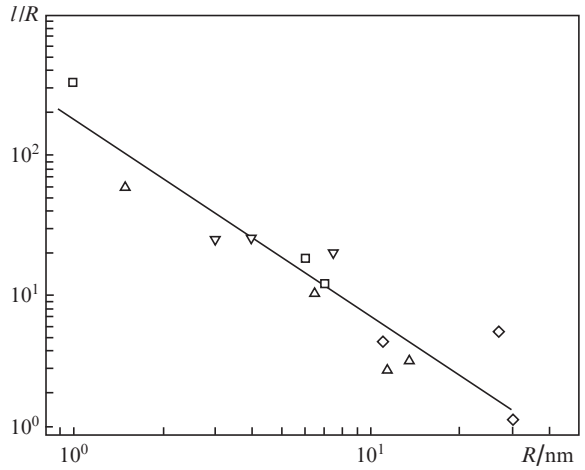

Figure 7. Dependence of the ratio l/R on the grain size for $Y_3Al_5O_{12}$ samples from Table 2 at $T = 3.86$ K.

The authors of [55] theoretically analysed the diffusive propagation of 0.874-THz phonons in dense α-Al_2O_3 ceramics with zero-thick boundaries, where the phonon scattering was caused only by the disorientation of crystallites (grains) in combination with their elastic anisotropy. The expression for the phonon free path given in [55] has the form $l = l_0(1 - \langle\cos\alpha\rangle)^{-1}$, where $\langle\cos\alpha\rangle$ is the average cosine of the angle of single scattering. This expression reflects the fact that the appearance of stresses with increasing size of grains and, as a result, the anisotropy in the grain structure lead to a decrease in the effective phonon free path (Fig. 7) and to a pulling of the trailing edge of recorded signals (Fig. 6). The above facts indirectly point to an enhancement of stresses with increasing grain size in the absence of twinning in the grain structure, which can be related to more severe conditions of compaction and synthesis and leads to a deterioration of thermophysical and optical characteristics (depolarisation) of the material.

The twinning processes may lead to a better structure [62, 63], because the formation of defects and their existence in small volumes are energetically unfavourable, and defects are carried out to the boundaries, which serve as defect sinks. The defects creating stresses of opposite signs can be drawn from neighbouring regions to the twin boundaries and annihilate there. Therefore, the structure of individual grains in such materials is obviously more perfect, i.e., the twinning boundary during its movement may efficiently clear the crystal from defects without making a noticeable contribution to phonon scattering. Table 3 lists the calculated lattice energies of initial single crystals and the energies of lattices with (111) [112] twins, which made it possible to estimate the twinning energy, and presents the microhardness of initial samples.

The twinning ability of crystals may also be responsible for solid-state reactions occurring during powdering of corresponding products [64]. The role played by twinning in the synthesis of $Y_3Al_5O_{12}$ laser ceramics from Al_2O_3 and Y_2O_3 powders is considered in [65].

Another example of a positive role of plastic deformation by twinning is a decrease in the number of dislocations and an improvement of the quality of the grain structure in optically transparent laser ceramics based on lithium fluoride [66].

8. Specific features of phonon spectra in nanostructured ceramics ($qR \sim 1$)

One of the trends in the development of ceramics technology is the use of nanostructured instead of microstructured materials. Our investigations showed that ceramic materials with the grain size $R < 100$ nm have weakly stabilised boundaries. A decrease in the grain size is related, as a rule, to a lower temperature and a shorter time of the synthesis, which leads to an increase in the thickness, a decrease in the density, and deterioration of elastic characteristics of the intergrain layer, which, in turn, results in deterioration of the thermophysical properties of the material.

Figure 8 shows the dependences $D(R)$ for standard Al_2O_3 and $ZrO_2:Y_2O_3$ ceramics [50], which are the extensions of the $D(R)$ dependences shown in Fig. 2 to the region of smaller R. The steep fall of the $D(R)$ dependence corresponding to $qR \approx 20$ can be considered as a restriction on the grain size imposed in view of optimisation of the thermophysical properties of dielectric oxide ceramics produced by compaction with subsequent annealing. This fall can be a beginning of the right wing of resonant phonon scattering from grains, which is confirmed by its shift to smaller R according to the difference in the velocities of sound ($v_{Al_2O_3} > v_{YSZ}$). The authors of [67] managed to create the condition $qR \sim 1$ and find a gap in the phonon spectrum of multiphase ceramics based on the $YSZ:Al_2O_3$ composite, which, in addition to the main fraction of YSZ crystallites, contains some amount (10%–15%) of nanosized ($R = 20$–40 nm) metastable Al_2O_3 phase.

It was shown that the position of the upper edge of the gap in the phonon spectrum is to a large extent determined by the

Table 3. Calculated lattice energies of initial single crystals and crystals with twins.

Crystal	Hardness/ GPa	Lattice energy (tabulated)/eV	Lattice energy (calculated)/eV	Lattice energy with twins/eV	Energy difference (%)	Twin energy/eV
$Lu_3Al_5O_{12}$	16.5	625.66	625.65	602.64	3.7	23.01
$Y_3Al_5O_{12}$	14	620.2	620.11	589.90	4.9	30.21
Lu_2O_3	9	142.2	139.98	135.82	3.0	4.16
Y_2O_3	8	133.4	131.42	122.67	6.7	8.75
MgO	6	41.2	41.38	41.13	0.6	0.25
LiF	1	10.56	10.61	10.46	1.4	0.15
NaF	0.65	9.46	9.43	9.35	0.9	0.08
NaCl	0.25	7.93	7.94	7.90	0.5	0.04

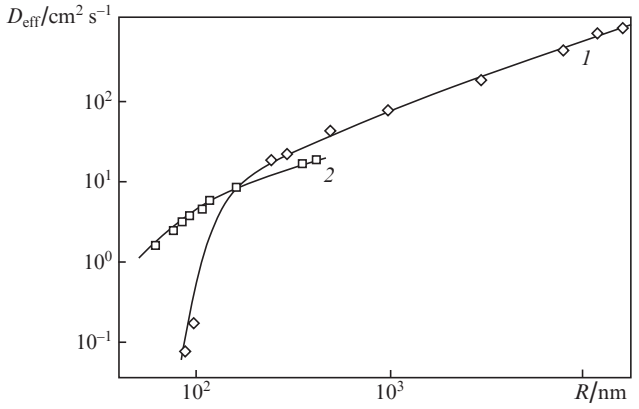

Figure 8. Dependences $D(R)$ for ceramics based on Al_2O_3 (*1*) and $ZrO_2:Y_2O_3$ (*2*).

elastic characteristics of the intergrain layer, while the presence of inclusions (pores, inclusions of another phase) with a characteristic size smaller than the grain size of the basic material of ceramics leads to a shift of the gap to the high-frequency region of the phonon spectrum.

9. Conclusions

Thus, investigation of the phonon kinetics in the region of liquid-helium temperatures is a sensitive method of comparative estimation of the degree of stabilisation of intergrain boundaries in ceramic materials depending on the conditions of their compaction and synthesis. The estimates of the thermophysical properties of ceramic materials reflect the average data on the acoustic impedance and the structure of intergrain boundaries in the samples. The plastic deformation by twinning in the grain structure makes it possible to improve the thermophysical and optical characteristics of ceramics.

The best quality of the intergrain boundaries, the absence of stresses in the grain structure, ordering of grains, and, as a result, the best acoustic, thermophysical, and optical properties are realised in $Nd^{3+}:Y_3Al_5O_{12}$ ceramics synthesised by sedimentation with the use of vacuum sintering in the absence of external pressure under the conditions when the main plastic deformation mechanism responsible for the formation of ceramic structure is twinning and the average grain size does not exceed 1–2 μm.

The acoustic transparency of $Y_3Al_5O_{12}$ oxide ceramics with twinning elements in its structure in the terahertz frequency region is comparable with the transparency of single crystals of $Ln^{3+}:Y_3Al_5O_{12}$ solid solutions. It is shown that, in the region of liquid helium temperatures, the ratio of the phonon free paths to the average grain size (l/R) can comprise several hundreds, which testifies to the crystallographic nature of intergrain boundaries, as well as to the absence of defects and defect-induced stresses in the grain structure.

The restrictions imposed on the grain size in oxide nanostructured ceramics in view of their thermophysical properties, which are related to possible resonant phonon scattering, are analysed. The possibility of formation of a gap in the phonon spectrum is to a large extent determined by the elastic properties of the intergrain layer, while the presence of inclusions (pores, inclusions of another phase) with a characteristic size smaller than the grain size of the basic material of ceramics leads to a shift of the gap to the high-frequency region of the phonon spectrum.

Acknowledgements. This work was done according to the Fundamental Research Plan of the A.V. Shubnikov Institute of Crystallography and the V.A. Kotel'nikov Institute of Radio Engineering and Electronics, Russian Academy of Sciences, and was partially supported by the Program of the President of the Russian Federation for Support of Leading Scientific Schools (Grant No. NSh-4732.2012.9), by the Program of the Presidium of the Russian Academy of Sciences 'Extreme optical fields and their application', and by grants of the Russian Foundation for Basic Research. The authors thank H. Yagi and T. Yanagitani (Konoshima Chemical Co., Japan), as well as V.V. Kravchenko and Yu.L. Kopylov (Institute of Radio Engineering and Electronics, Russian Academy of Sciences, Fryazino branch) for the samples of ceramics.

References

1. Lu J., Ueda K., Yagi H., Yanagitani T., Akiyama Y., Kaminskii A.A. *J. Alloys Compd.*, **341**, 220 (2002).
2. Ikesue A., Aung Y.I., Taira T., Kamimura T., Yoshida K., Messing G. *Ann. Rev. Mat. Res.*, **36**, 397 (2006).
3. Kaminskii A.A. *Laser. Photon Rev.*, **1**, 93 (2007).
4. Taira T. *Rev. Laser Eng.*, **37**, 227 (2009).
5. Sanghera J., Kim W., Villaiobos G., Shaw B., Baker C., Frantz J., Sadowski B., Aggarwal I. *Materials*, **5**, 258 (2012).
6. Ter-Gabrielyan N., Merkle L.D., Ikesue A., Dubinskii M. *Opt. Lett.*, **33**, 1524 (2008).
7. Lu J., Bisson J.F., Takaichi K., Uematsu T., Shirakawa A., Musha M., Ueda K., Yagi H., Yanagitani T., Kaminskii A.A. *Appl. Phys. Lett.*, **83**, 1101 (2003).
8. Lu J., Murai T., Takaichi K., Uematsu T., Ueda K., Yagi H., Yanagitani T., Kaminskii A.A. *Jpn. J. Appl. Phys.*, **41**, L1277 (2001).
9. Newburgh G.A., Sor-Daniels A., Michel A., Merkle L.D., Ikesue A., Dubinskii M. *Opt. Express*, **19**, 3604 (2011).
10. Ter-Gabrielyan N., Merkle L.D., Newburgh G.A., Dubinskii M. *Laser Phys.*, **19**, 867 (2009).
11. Sanamyan T., Simmons J., Dubinskii M. *Laser Phys. Lett.*, **7**, 569 (2010).
12. Lu J., Takaichi K., Uematsu T., Shirakawa A., Musha M., Ueda K., Yagi H., Yanagitani T., Kaminskii A.A. *Jpn. J. App. Phys.*, **41**, L1373 (2001).
13. Greskovich C., Chernoch J.P. *J. App. Phys.*, **44**, 4599 (1973).
14. Strohmaier S.G.P., Eichler H.J., Bisson J.-F., Yagi H., Takaichi K., Ueda K., Yanagitani T., Kaminskii A.A. *Laser Phys. Lett.*, **2**, 383 (2005).
15. Ikesue A., Kinoshima T., Kamata K., Yoshida K. *J. Am. Ceram. Soc.*, **78**, 1033 (1995).
16. Lu J., Shirakawa A., Ueda K., Yagi H., Yanagitani T., Gabler V., Eichler H.J., Kaminskii A.A. *Phys. Status Solidi A*, **189**, R11 (2002).
17. Cheng X.J., Xu J.Q., Wang M.J., Jiang B.X., Zhang W.X., Pan Y.B. *Laser Phys. Lett.*, **7**, 351 (2010).
18. Ter-Gabrielyan N., Merkle L.D., Kupp E.P., Messing G.L., Dubinskii M. *Opt. Lett.*, **35**, 922 (2010).
19. Zhang W.X., Pan Y.B., Zhou J., Liu W.B., Li J., Jiang B.X., Cheng X.J., Xu J.Q. *J. Am. Ceram. Soc.*, **92**, 2434 (2009).
20. Takaichi K., Yagi H., Lu J.K., Shirakawa A., Ueda K., Yanagitani T., Kaminskii A.A. *Phys. Status Solidi A*, **200**, R5 (2003).
21. Sato Y., Saikawa J., Shoji I., Taira T., Ikesue A. *J. Ceram. Soc. Jpn.*, **112**, S313 (2004).
22. Saikawa J., Sato Y., Taira T., Ikesue A. *Appl. Phys. Lett.*, **85**, 1898 (2004).
23. Kaminskii A.A., Bagaev S.N., Ueda K., Yagi H., Eichler H.J., Shirakawa A., Tokurakawa M., Rhee H., Takaichi K., Yanagitani T. *Laser Phys. Lett.*, **6**, 671 (2009).
24. Kaminskii A.A., Bagaev S.N., Ueda K., Takaichi K., Lu J., Shirakawa A., Yagi H., Yanagitani T., Eichler H.J., Rhee H. *Laser Phys. Lett.*, **2**, 30 (2005).

25. Lu J.. Takaichi K., Uematsu T., Shirakawa A., Musha M., Bisson J.F., Ueda K., Yagi H., Yanagitani T., Kaminskii A.A. *Laser Phys*., **13**, 940 (2003).
26. Kaminskii A.A., Kurakawa H., Shirakawa A., Ueda K., Tanaka N., Becker P., Bohatý L., Akchurin M., Tokurakawa M., Kuretake S., Kintaka Y., Kageyama K., Takagi H. *Laser Phys. Lett*., **6**, 304 (2009).
27. Lu J., Takaichi K., Uematsu T., Shirakawa A., Musha M., Ueda K., Yagi H., Yanagitani T., Kaminskii A.A. *Appl. Phys. Lett*., **81**, 4324 (2002).
28. Antipov O.L., Novikov A.A., Zakharov N.G., Zinoviev A.P. *Opt. Mater. Lett*., **2**, 183 (2012).
29. Tokurakawa M., Takaichi K., Shirakawa A., Ueda K., Yagi H., Hosokawa S., Yanagitani T., Kaminskii A.A. *Opt. Express*, **14**, 12832 (2006).
30. Xu C.W., Luo D.W., Zhang J., Yang H., Qin X.P., Tan W.D., Tang D.Y. *Laser Phys. Lett*., **9**, 30 (2012).
31. Basiev T.T., Doroshenko M.E., Fedorov P.P., Konyushkin V.A., Kuznetsov S.V., Osiko V.V., Akchurin M.Sh. *Opt. Lett*., **33**, 521 (2008).
32. Basiev T.T., Konyushkin V.A., Konyushkin D.V., Dorioshenko M.E., Huber G., Reichert F., Hansen N.O., Fechner M. *Opt. Mater. Express*, **1**, 1511 (2011).
33. Basiev T.T., Doroshenko M.T., Konyushkin V.A., Osiko V.V. *Opt. Lett.*, **35** (23), 4009 (2010).
34. Aklyama J., Sato Y., Taira T. *Appl. Phys. Express*, **4**, 022703 (2011).
35. Kaminskii A.A., Akchurin M.Sh., Gainutdinov R.V., Takaichi K., Shirakawa A., Yagi H., Yanagitani T., Ueda K. *Krystallografiya*, **50**, 935 (2005).
36. Taira T., Ikesue A., Yoshida K., in *Adv. Solid-State Lasers OSA TOPS*, **19**, 430 (1998).
37. Lu J., Prabhu M., Xu J., Ueda K., Yagi H., Yanagitani T., Kaminskii A.A. *Appl. Phys. Lett*., **77**, 3707 (2000).
38. Lu J., Murai T., Uematsu T., Misawa K., Prabhu M., Xu J., Ueda K., Yagi H., Yanagitani T., Kaminskii A.A., Kudryashov A. *Appl. Phys. Lett*., **78**, 3586 (2001).
39. Lu J., Murai T., Takaichi K., Misawa K., Prabhu M., Xu J., Ueda K., Yagi H., Yanagitani T., Kudryashov A., Kaminskii A.A. *Laser Phys*., **11**, 1053 (2001).
40. Sekita M., Hanada H., Yanagitani T., Shirasaki S. *J. Appl. Phys*., **67**, 453 (1990).
41. Yanagitani T., Yagi H., Ichikawa M. Japanese Patent 10-101333 (1998); Yanagitani T., Yagi H., Hiro Y. Japanese Patent 10-101411 (1998).
42. Clarke D.R. *J. Am. Ceram. Soc*., **70** (1), 15 (1987).
43. Ernst P., Kienzle O., Ruhle M. *J. Europ. Ceram. Soc*., 19 (6–7), 665 (1999).
44. Von Gutfeld R.J., Nethercot Jr. A.H. *Phys. Rev. Lett*., **12** (23), 641 (1964).
45. Levinson I.B. *Zh. Eksp. Teor. Fiz*., **79** (10), 1394 (1980).
46. Ivanov S.N., Khazanov E.N., Paszkiewicz T., Wilczynski M., Taranov A.V. *Z. Phys. B*, **99** (4), 535 (1996).
47. Yagi H., Yanagitani T., Numazawa T., Ueda K. *Ceramics International*, **33**, 711 (2007).
48. Ivanov S.N., Kozorezov A.G., Taranov A.V., Khazanov E.N. *Zh. Eksp. Teor. Fiz*., **102** (8), 600 (1992).
49. Barabanenkov Yu.N., Ivanov V.V., Ivanov S.N., Taranov A.V., Khazanov E.N. *Zh. Eksp. Teor. Fiz*., **119** (3), 546 (2001).
50. Barabanenkov Yu.N., Ivanov V.V., Ivanov S.N., Salamatov E.I., Taranov A.V., Khazanov E.N., Khasanov O.L. *Zh. Eksp. Teor. Fiz.*, **129** (1), 131 (2006).
51. Ivanov V.V., Ivanov S.N., Kaigorodov A.S., , Taranov A.V., Khazanov E.N., Khrustov V.R. *Neorg. Mater*., **43** (12), 1515 (2007).
52. Ivanov V.V., Ivanov S.N., Karban' O.V., Taranov A.V., Khazanov E.N., Khrustov V.R. *Neorg. Mater.*, **40** (11), 1400 (2004).
53. Barabanenkov Yu.N., Ivanov S.N., Taranov A.V., Khazanov E.N., Yagi H., Yanagitani T., Takaichi K., Lu J., Bisson J.F., Shirakawa A., Ueda K., Kaminskii A.A. *Pis'ma Zh. Eksp. Teor. Fiz*., **79** (7), 421 (2004).
54. Kagan V.D., Suslov A.V. *Fiz. Tv. Tela*, **36** (9), 2672 (1994).
55. Kaplyanskii A.A., Mel'nikov M.B., Feofilov S.N. *Fiz. Tv. Tela*, **38** (5), 1434 (1996).
56. Taranov A.V., Khazanov E.N. *Zh. Eksp. Teor. Fiz.*, **134** (9), 595 (2008).
57. Kaminskii A.A., Bagayev S.N., Ueda K., Takaichi K., Shirakawa A., Ivanov S.N., Khazanov E.N., Taranov A.V., Yagi H., Yanagitani T. *Laser Phys. Lett*., **3** (8), 375 (2006).
58. Akchurin M.Sh., Zakalyukin R.M. *Kristallografiya*, **51** (6), 1059 (2006).
59. Akchurin M.Sh., Gainutdinov R.V., Zakalyukin R.M., Kaminskii A.A. *Doklady Akad. Nauk*, **415** (3), 322 (2007).
60. Akchurin M.Sh., Gainutdinov R.V., Kaminskii A.A., Taranov A.V., Khazanov E.N. *Zh. Eksp. Teor. Fiz*., **135** (1), 93 (2009).
61. Solov'eva A.E. *Neorg. Mater.*, **21** (5), 808 (1985).
62. Akchurin M.Sh., Gainutdinov R.V., Kaminskii A.A. *Poverkhn. Rentgen., Sinkhrotron., Neitron. Issl.*, **9**, 78 (2006).
63. Akchurin M.Sh., Galiulin R.V. *Kristallografiya*, **43** (3), 493 (1998).
64. Akchurin M.Sh., Gainutdinov R.V., Kupenko I.I., Yagi H., Ueda K., Shirakawa A., Kaminskii A.A. *Doklady Akad. Nauk*, **441** (6), 743 (2011).
65. Akchurin M.Sh., Zakalyukin R.M., Kaminskii A.A. *Doklady Akad. Nauk*, 2012 (in press).
66. Khazanov E.N., Taranov A.V., Gainutdinov R.V., Akchurin M.Sh., Basiev T.T., Konyushkin V.A., Fedorov P.P., Kuznetsov S.V., Osiko V.V. *Zh. Eksp. Teor. Fiz*., **137** (6), 1126 (2010).
67. Ivanov V.V., Salamatov E.I., Taranov A.V., Khazanov E.N., *Zh. Eksp. Teor. Fiz*., **133** (2), 339 (2008).